PHYSICAL REVIEW D VOLUME 18, NUMBER 7 1 OCTOBER 1978

Pion-quark scattering model for lepton pair production*

Christopher M. Debeau and Dennis Silverman
Department of Physics, University of California, Irvine, Irvine, California 92717
(Received 24 June 1977; revised manuscript received 19 September 1977)

A model for lepton pair production from quark-antiquark annihilation is presented in which antiquarks are obtained from constituent pions and form factors are included to account for the transverse-momentum dependence. The single-lepton spectrum and the lepton-pair spectra in mass squared, transverse momentum, and longitudinal momentum are calculated and compared with proton- and pion-beam experiments.

I. INTRODUCTION

Experiments have recently studied the spectrum of lepton pairs emitted in hadron collisions. These[1-3] have varied all of the parameters of the pairs: mass squared, $0.04 \leq Q^2 \leq 120$ GeV^2; transverse momentum, $0 \leq Q_\perp \leq 5$ GeV/c; and Feynman-scaled longitudinal momentum, $0 \leq x_F \leq 1$. Some experiments[2,3] have also included pion beams. These are complemented by experiments[4] which measure the single-lepton spectrum and go to larger $q_\perp \lesssim 6$ GeV/c. In this paper we attempt to fit the continuum contribution to these processes with a model that is basically the Drell-Yan model[5]: quark-antiquark annihilation to a lepton pair via a virtual photon. To account for the $Q_\perp$ dependence we modify the Drell-Yan model by using constituent pions as the source of antiquarks or sea quarks[6] and incorporate the transverse-momentum and related off-mass-shell dependence of the quarks in terms of a form factor describing the meson wave function.

The Drell-Yan process as originally calculated uses on-mass-shell quark constituents of only the initial beams and yields a single-lepton spectrum that falls off with the canonical scaling power $q_\perp^{-4}$. This has been compared with data[7,8] and found to be an order of magnitude smaller, although approaching the data at the largest $q_\perp \sim 6$ GeV/c. Since the μ/π spectrum ratio is approximately constant in $q_\perp$, the single-lepton spectrum must fall faster in $q_\perp$. This same situation arises with the single-pion spectrum falling as $q_\perp^{-8}$ instead of the canonical $q_\perp^{-4}$ scaling behavior. In order to provide a mechanism for this canonical scaling violation we introduce constituent pions as the predominant source of sea antiquarks[6] or quarks and include a form factor $F_\pi(k^2)$ for the pion to dissociate to an off-shell quark or antiquark with virtual momentum squared k^2 (Fig. 1). This quark exchange also provides the scattering mechanism which creates virtual photons with momentum transverse to the beam or collinear constituent pion direction.

In the modified Drell-Yan model, the high-$Q_\perp$ lepton pair requires that an annihilating quark or antiquark have a high $k_\perp = Q_\perp$, and this is the exchanged quark in Fig. 1. This high-$k_\perp$ quark is also off its mass shell by an order $k^2 \sim -k_\perp^2$. The form factor $F_\pi(k^2) = A(-k^2 + m^2)^{-1/2}$ is used (with A having the dimensions of mass) for the off-shell quark or antiquark in a pion. This describes effectively the distribution of quark transverse momentum and provides the extra damping in $k_\perp$ needed to agree with experiment.

The constituent pions are considered to have a central plateau or sea-type distribution $P_{\pi/p} = (2.5/x)(1-x)^7$. Pion-beam experiments are also studied with the same model (Fig. 2). The valence q and $\bar{q}$ in the pion are also supplemented by a sea resulting from pion constituents of the pion $P_{\pi/\pi} = 2/3(2.5/x)(1-x)^7$.

The power in $F_\pi(k^2)$ is chosen to be consistent

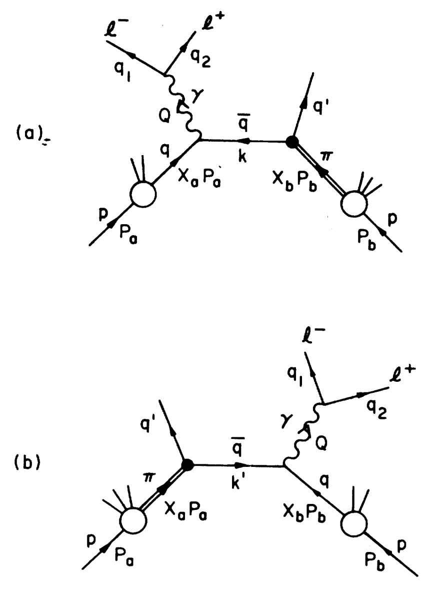

FIG. 1. (a) Direct and (b) crossed diagrams for $pp \to l^+ l^- X$ via secondary-pion–quark scattering with quark interchange.

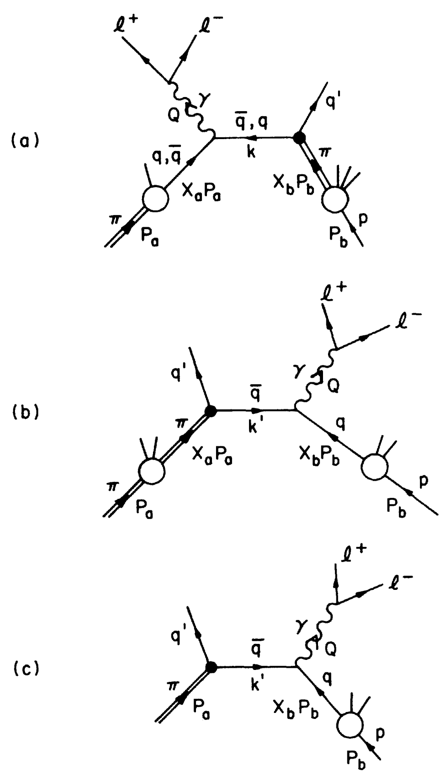

FIG. 2. (a) Direct and (b) crossed diagrams for secondary-pion–quark scattering for pion beams in $\pi p \to l^+ l^- X$ and (c) initial-pion diagram.

with the constituent-interchange calculation of the calculation of the single-pion spectrum via $q+\pi \to \pi + q$ (Fig. 3). There the form factor occurs twice in the amplitude giving the $E d\sigma/dp^3 \propto A^4 p_\perp^{-8}$ behavior of the cross section at CERN ISR. Here the analogous process (Fig. 1) for lepton pair production has $F_\pi(k^2)$ occurring only once in the amplitude. This gives for the single-lepton spectrum $q^0 d\sigma/dq^3 \propto A^2 q_\perp^{-6}$. Since m^2 is large, however, the l/π ratio does not show significant deviation from a constant until $q_\perp \gtrsim 4$ GeV/c.

The coupling strength A and mass m are adjusted to fit the data, and good agreement is found between the A needed for lepton production experiments and the single-pion spectrum.

In Sec. II we present the detailed calculations of the model and in Sec. III we compare the numerical results with the experiments.

II. PAIR CREATION IN MESON-QUARK SCATTERING

The modified Drell-Yan model calculates lepton pair creation from scattering of quark-meson constituents. As seen in Fig. 1, the quarks and pion are treated as constituent partons with fractional momenta x_a, x_b and probability distributions $P_{q/p}(x_a)dx_a$, $P_{\pi/p}(x_b)dx_b$, respectively. The quark and antiquark annihilate to form a virtual photon of momentum Q^μ and mass squared Q^2. Although the transverse momentum of the constituents is small and has been neglected, photons at nonzero $Q_\perp$ can be produced due to the interchanged antiquark with $k_\perp = Q_\perp$. If we view this in the standard Drell-Yan way, the pion is actually providing an intermediate link for calculating the effective transverse-momentum distribution of antiquarks from a proton.[7,8] Such a source of $Q_\perp$ dependence is necessary to fit cross sections such as $d\sigma/dQ^2 dQ_\perp^2$ since the standard Drell-Yan calculation

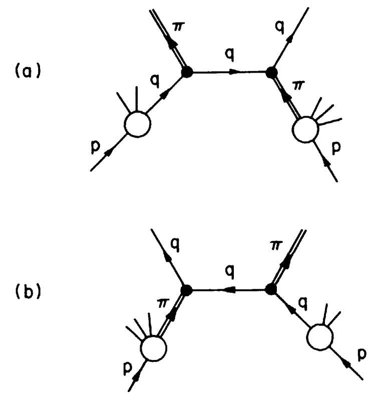

FIG. 3. Direct and crossed diagrams for secondary-pion–quark scattering in $pp \to \pi X$ via constituent interchange.

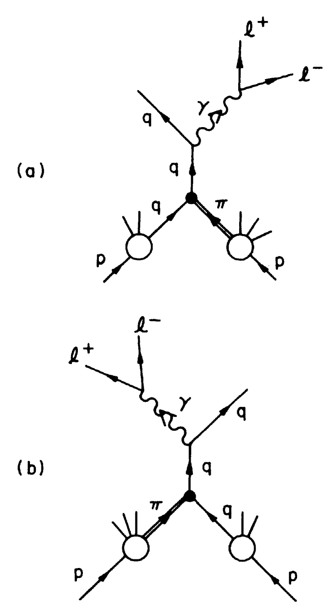

FIG. 4. Quark bremsstrahlung or s-channel quark diagrams for $pp \to l^+ l^- X$ via secondary-pion–quark scattering.

creates virtual photons at $Q_\perp = 0$.

The off-shell quark exchange Fig. 1(a) is not by itself gauge invariant. Including the s-channel quark pole in Fig. 4(a) does not make it gauge invariant due to the form factors at the pion vertices. The form factors mean that the pion vertex contains an internal structure, and the virtual photon must be coupled to the internal charges. However, we can isolate the contribution that this vertex adds to the quark s- and t-channel poles to make a gauge-invariant amplitude.[9] The current from Fig. 1(a) is

$$j_q^\mu = e\lambda_q \bar{u}(q')\gamma_5 F_\pi(k^2)(-\not{k} - m)^{-1}\gamma^\mu u(x_a P_a)\,.$$

The current of the virtual photon coupling into the $\pi_{q\bar{q}}$ vertex itself has several Lorentz-covariant terms, among which we need only

$$j_v^\mu = e\bar{u}(q')\gamma_5 Q^\mu u(x_a P_a) f(\hat{s}, k^2; Q^2)\,,$$

where $\hat{s} = (x_a P_a + x_b P_b)^2$. The amplitude f necessary to make $j = j_q + j_v$ gauge invariant is obtained from setting $Q\cdot(j_q + j_v) = 0$, giving $f = \lambda_q F_\pi(k^2)/Q^2$ and

$$j^\mu = e\lambda_q \bar{u}(q')\gamma_5 F_\pi(k^2) \times [(-\not{k} - m)^{-1}\gamma^\mu + Q^\mu/Q^2]u(x_a P_a)\,.$$

Since the added Q^μ vertex term is contracted with the current-conserving lepton current it contributes nothing to the cross section and will henceforth be dropped. The crossed diagram Fig. 1(b) and the s-channel pole terms Fig. 4 are made gauge invariant in the same way with the Q^μ vertex terms.

The differential cross section for the pair creation process direct graph [Fig. 1(a)] is

$$d\sigma = \tfrac{1}{3}\int dx_a \int dx_b P_{q/p}(x_a) P_{\pi/p}(x_b) \frac{1}{4x_a P_a^0 x_b P_b^0 V_{\rm rel}(2\pi)^5} \frac{d^3q_1}{2q_1^0}\frac{d^3q_2}{2q_2^0}\frac{d^3q'}{2q_0'}\delta^4(x_a P_a + x_b P_b - q_1 - q_2 - q')F_\pi^2(k^2)$$
$$\times \tfrac{1}{2}\sum_{\rm spins}\left|\bar{u}(q\ )\gamma_\mu v(q_2)\frac{e^2\lambda_q}{Q^2}\bar{u}(q')\gamma_5\frac{(-\not{k}+m)}{k^2-m^2}\gamma^\mu u(x_a P_a)\right|^2,$$

where m is the effective quark mass, $e\lambda_q$ is the quark charge, $Q = q_1 + q_2$, $k = Q - x_a P_a$, and $\frac{1}{3}$ is included for color. The crossed graph, Fig. 1(b), is obtained from this by interchanging $x_a \leftrightarrow x_b$, $P_a \leftrightarrow P_b$, and thereby $k^2 = (Q - x_a P_a)^2$ to $k'^2 = (Q - x_b P_b)^2$. This expression is summed over all consistent quark and pion charges. Also included are antiquark sea distributions in the proton coupled with quarks from pions, which are important at low Q^2. For all subsequent cross sections, the d^3q' integral is evaluated using the momentum δ functions, and then the x_b integral is evaluated by the energy δ function

$$\int dx_b \frac{1}{2q_0'}\delta(x_a P_a^0 + x_b P_b^0 - Q^0 - q_0') = \int dx_b \delta((x_a P_a + x_b P_b - Q)^2 - q'^2)$$
$$= \frac{x_b}{-k^2 + m^2 + x_b^2 m_b^2}\,,$$

where x_b is related to x_a and Q from the δ function condition

$$x_a x_b(s - m_a^2 - m_b^2) - 2x_a P_a\cdot Q - 2x_b P_b\cdot Q + Q^2 = m^2 - x_a^2 m_a^2 - x_b^2 m_b^2\,. \tag{2.2}$$

This kinematics yields

$$\frac{x_a dx_b}{-k'^2 + m^2 + x_a^2 m_a^2} = \frac{x_b dx_a}{-k^2 + m^2 + x_b^2 m_b^2}\,. \tag{2.3}$$

For calculating the single-muon spectrum with q_1 observed and q_2 integrated over we find

$$q_1^0\frac{d\sigma}{d^3q_1} = \frac{\lambda_q^2}{3}\frac{\alpha^2}{\pi^3 s}\int\frac{d^3q_2}{q_2^0}\int_{x_0}^1 dx_a P_{q/p}(x_a)\frac{P_{\pi/p}(x_b)x_b}{(-k^2+m^2+x_b^2m_b^2)}$$
$$\times\frac{q_1\cdot P_a q_2\cdot P_b + q_2\cdot P_a q_1\cdot P_b}{(Q^2)^2}\frac{F_\pi(k^2)^2}{(-k^2+m^2)} + \text{crossed}\,, \tag{2.4}$$

where

$$x_0 = \frac{2P_b\cdot Q - Q^2 - m_b^2 - m_a^2 x_0^2 + W_b^2}{2P_a\cdot P_b - 2P_a\cdot Q}\,. \tag{2.5}$$

W_b is the threshold energy for the system of the fragmented proton plus quark in $P_b - k$. We use $W_b = m_p + m$. The limit on the $|\bar{q}_2|$ integral is

$$|\bar{q}_2| \leq \frac{\sqrt{s}/2 - |\bar{q}_1|}{1-(1-\cos\theta_{12})|\bar{q}_1|/\sqrt{s}}\,.$$

The diffferential cross section for massive muon pairs $Q^0 d\sigma/dQ^2 d^3Q$ is obtained from above by inserting $\int d^4Q\,\delta^4(Q - q_1 - q_2)$, integrating over q_1 instead of Q, and converting $2Q^0dQ^0 = d(Q^2)$. The d^3q_2 integral is evaluated with $\delta^3(\overline{Q} - \bar{q}_1 - \bar{q}_2)$. The only dependence on q_1 and q_2 separately from Q is then in

$$\int \frac{d^3q_1}{q_1^0 q_2^0}\delta(Q^0 - q_1^0 - q_2^0)(q_1\cdot P_a q_2\cdot P_b + q_2\cdot P_a q_1\cdot P_b) = \frac{\pi}{3}\,[2(Q\cdot P_a Q\cdot P_b) + Q^2 P_a\cdot P_b]$$

$$= \frac{\pi}{6}\,s(Q_\perp{}^2 + 2Q^2)\,, \tag{2.6}$$

where we have dropped the lepton mass. We then have

$$\frac{Q^0 d\sigma}{d(Q^2)d^3Q} = \frac{\lambda_q{}^2}{3}\,\frac{\alpha^2}{12\pi^2}\,\frac{Q_\perp{}^2 + 2Q^2}{(Q^2)^2}\left[\int_{x_0}^1 dx_a \frac{x_b P_{q/p}(x_a) P_{\pi/p}(x_b)}{(-k^2 + m^2 + x_b{}^2 m_b{}^2)}\,\frac{F_\pi{}^2(k^2)}{(-k^2+m^2)}\right.$$

$$\left. + \int_{x_0'}^1 dx_b \frac{x_a P_{\pi/p}(x_a) P_{q/p}(x_b)}{(-k'^2 + m^2 + x_a{}^2 m_a{}^2)}\,\frac{F_\pi{}^2(k'^2)}{(-k'^2+m^2)}\right], \tag{2.7}$$

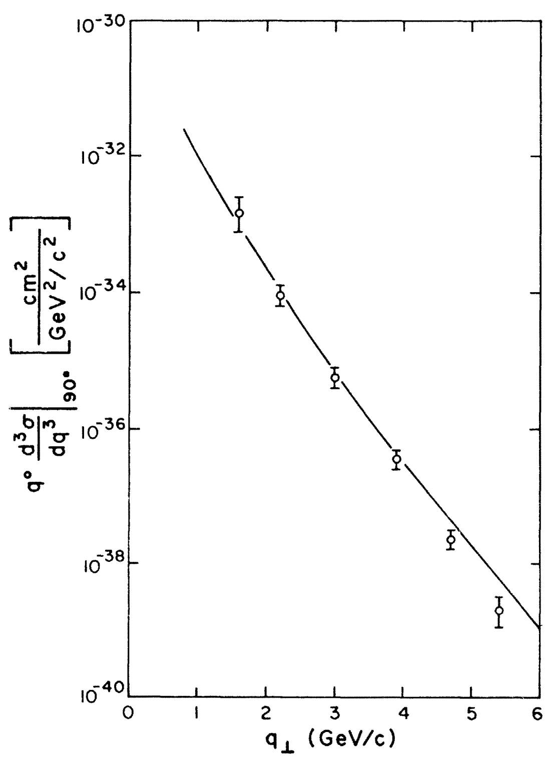

FIG. 5. $q^0 d^3\sigma/dq^3$ for single muons at 90° compared to the data of Boymond *et al.* (Ref. 4) at $\sqrt{s} = 23.7$ GeV.

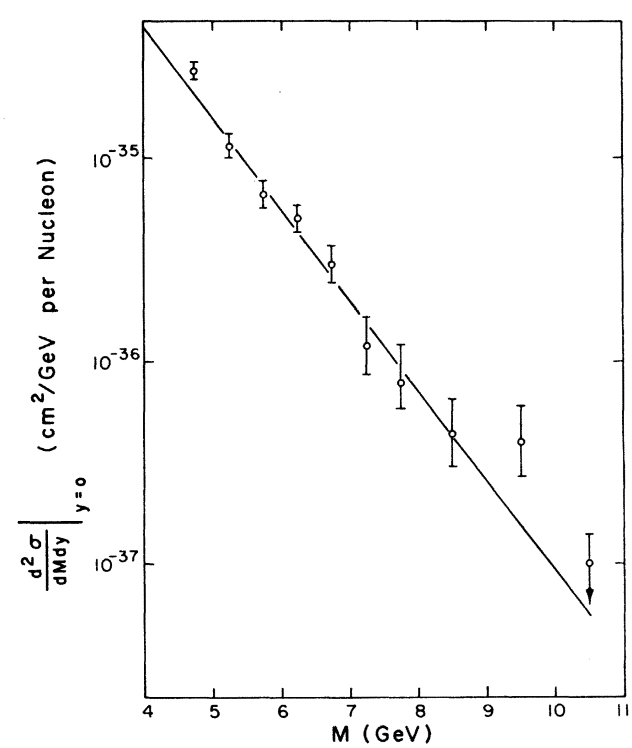

FIG. 6. $d^2\sigma/dMdy$ for muon pairs at $y = 0$ compared to the data of Hom *et al.* at $\sqrt{s} = 27.4$ GeV.

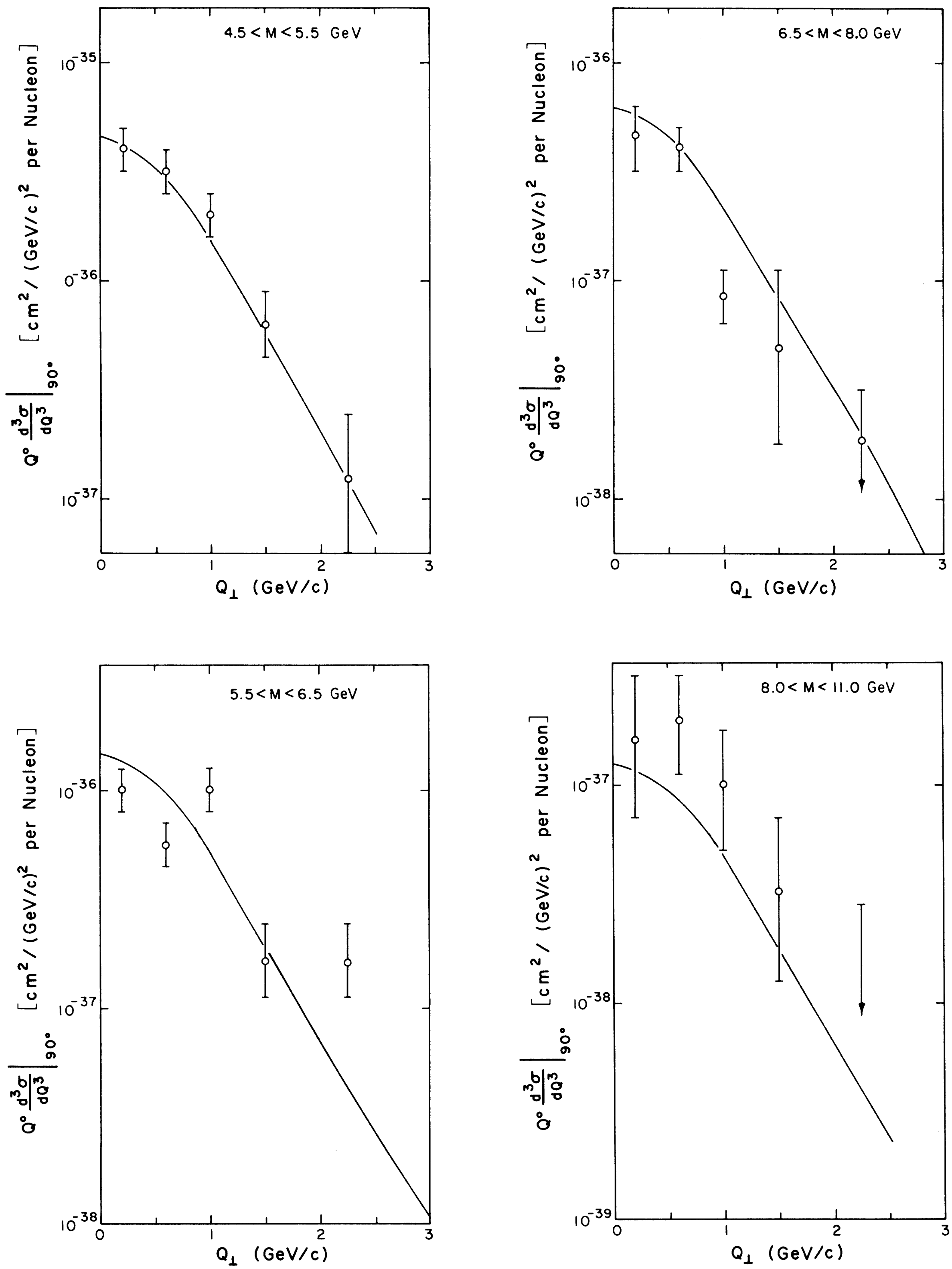

FIG. 7. $Q^0 d^3\sigma/dQ^3$ for muon pairs at 90° and $\sqrt{s}=27.4$ GeV. Compared to the data of Hom *et al.* (Ref. 4) for various mass bins.

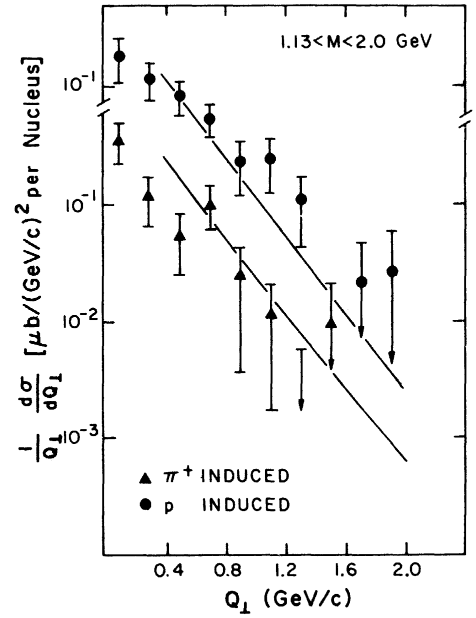

FIG. 8. $Q_\perp^{-1}d\sigma/dQ_\perp$ for muon pairs, per nucleus, for a Be target, for both incident proton and π^+ beams. Compared with the data of Anderson *et al*. (Ref. 2) at $\sqrt{s}=16.8$ GeV in a nonresonant mass bin.

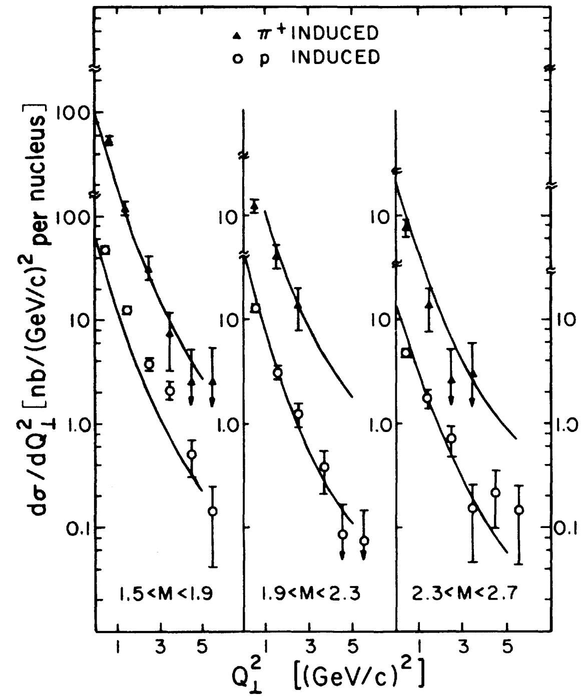

FIG. 10. $d\sigma/dQ_\perp^2$ for muon pairs, per nucleus, for a carbon target, for both incident proton and π^+ beams. Compared with the data of Anderson *et al*. (Ref. 3) at $\sqrt{s}=20.6$ GeV in various mass bins.

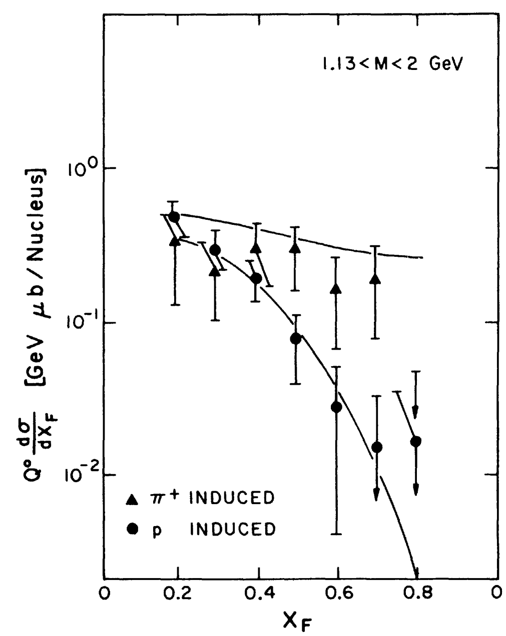

FIG. 9. $Q^0 d\sigma/dx_F$ for muon pairs, per nucleus, for a Be target, for both incident proton and π^+ beams. Compared with the data of Anderson *et al*. (Ref. 2) at $\sqrt{s}=16.8$ GeV in a nonresonant mass bin.

where x_0' is obtained from x_0 by interchanging a and b.

The $(-k^2+m^2)^{-1}$ factors in the propagator, kinematics, and form factor are largest at $x_a=x_0$. At 90° or $Q_z=0$ and $Q^0\ll s^{1/2}/2$, we have $(-k^2+m^2)\simeq(Q_\perp^2+m^2)$ and this determines the $Q_\perp$ dependence to be $\approx Q_\perp^{-4}$.

With pion beams, the direct graph has contributions $P_{q/\pi}(x_a)$ and $P_{\bar{q}/\pi}(x_a)$ from on-shell q or $\bar{q}$ [Fig. 2(a)] in place of $P_{q/p}(x_a)$ in the first term of Eq. (2.7). The cross graph [Fig. 2(b)] has $P_{\pi/\pi}(x_a)=1.7(1-x_a)^7/x_a$, a central plateau distribution which dominates low-x_F calculations. In addition, we can have the crossed type graph with the initial pion as the source of the off-shell antiquark instead of a secondary pion [Fig. 2(c)]. This is given by replacing $P_{\pi/\pi}(x_a)$ by $\delta(x_a-1)$ in the second term of Eq. (2.7) and retaining the $F_\pi(k'^2)$ off-shell form factor to allow it to contribute to $Q_\perp\neq 0$ lepton pairs. We have considered the diagram with a direct-channel quark pole[10] (Fig. 4) that would make a pointlike theory gauge invariant. The cross section with this s-channel quark propagator and pion form factor behaves like $A^2/\hat{s}^2$ with $\hat{s}=sx_ax_b$ and at 90°, $\hat{s}>\sqrt{s}\,(Q_\perp^2+Q^2)^{1/2}$. The quark-exchange t-channel diagrams (Fig. 1) that we have used behave like $A^2/(k^2)^2$, however, and are dominated by the smallest possible $k^2\simeq -Q_\perp^2$.

The s-channel quark diagrams are thus down by order $Q_\perp^2/s$ from the t-channel exchanges.

III. RESULTS

We determine the parameters for these calculations as follows. The proton quark distribution functions $P_{q/p}(x)$ are those which fit electroproduction and neutrino production.[11] The distribution functions for quarks in pions are taken to be[12] $P_{q/\pi}(x)=0.15/x$.

The secondary-pion distribution functions $P_{\pi/p}(x)$ are fitted to the pion spectra[13] at 90°,

$$P_{\pi^+/p}(x)=2.5\left[\frac{(1-x)^7}{x}+0.05(1-x)^5\right],$$
$$P_{\pi^-/p}(x)=2.5\left[\frac{(1-x)^7}{x}+0.05(1-x)^6\right],$$
$$P_{\pi^0/p}(x)=\tfrac{1}{2}(P_{\pi^+}+P_{\pi^-}), \tag{3.1}$$

and the normalization is chosen so that $xP_{\pi/p}(x)\to 2.5$ as $x\to 0$ gives the magnitude of the central plateau.

These functions also satisfy the sum rule

$$\sum_{\pi^\pm,\pi^0}\int_0^1 xP_{\pi/p}(x)\,dx \lesssim 1\,. \tag{3.2}$$

A. Single-lepton spectrum

We calculate $q^0d^3\sigma/dq^3$ for large transverse momentum muons at 90° and $\sqrt{s}=23.7$ GeV. We compare with the cross section per nucleon of Boymond *et al.*[4] for Cu and W targets and find that our calculation has the proper $q_\perp^{-8}$ dependence at large $q_\perp$ (Fig. 5). The data are fitted with $A=7.8$ GeV and $m^2=4$ GeV^2.[14]

B. Lepton-pair spectra at 90°

We calculate $d^2\sigma/dMdy$ per nucleon ($M^2=Q^2$) at $\sqrt{s}=27.4$ GeV and compare with Hom *et al.*[1] for Be and Cu targets (Fig. 6). We also integrate $Q^0d\sigma/dQ^3\,dQ^2$ over the mas bins and compare in Fig. 7 with $A=12.8$ GeV and $m^2=4$ GeV^2.

C. Lepton-pair spectra $x_F \neq 0$

We calculate $Q_\perp^{-1}d\sigma/dQ_\perp$ per nucleus, for a Be target, integrated over x_F for both incident proton and π^+ beams at $\sqrt{s}=16.8$ GeV (Fig. 8). We find good agreement with Anderson *et al.*[2] in the mass bin not dominated by a resonance $1.13<M<2.0$ GeV. In the other nonresonant mass bin $0.45<M<0.55$ GeV the data exceeds our calculation by an order of magnitude and indicate additional sources of lepton pairs for very low $Q^2<0.5$ GeV^2.

We also calculate $Q^0d\sigma/dx_F$ and compare with the same experiment in the same mass bin (Fig. 9). The flatness of the pion-beam produced pairs at

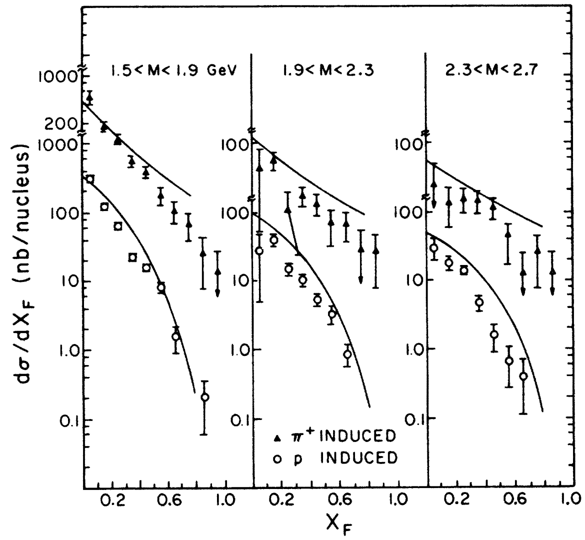

FIG. 11. $d\sigma/dx_F$ for muon pairs, per nucleus, for a carbon target, for both incident proton and π^+ beams. Compared with the data of Anderson *et al.* (Ref. 3) at $\sqrt{s}=20.6$ GeV in various mass bins.

$x_F>0.3$ is due to the pion beam directly producing an antiquark for the annihilation.

Calculations of $d\sigma/dQ_\perp^2$ (Fig. 10) and $d\sigma/dx_F$ (Fig. 11) per nucleus, for both incident proton and π^+ beams at $\sqrt{s}=20.6$ are found to be in agreement with Anderson *et al.*[3] in the nonresonant bins $1.5<M<1.9$, $1.9<M<2.3$, and $2.3<M<2.7$ GeV.

The data for the calculations in this subsection are fitted with $m^2=1$ GeV^2 and the normalization $A=12.8$ GeV.

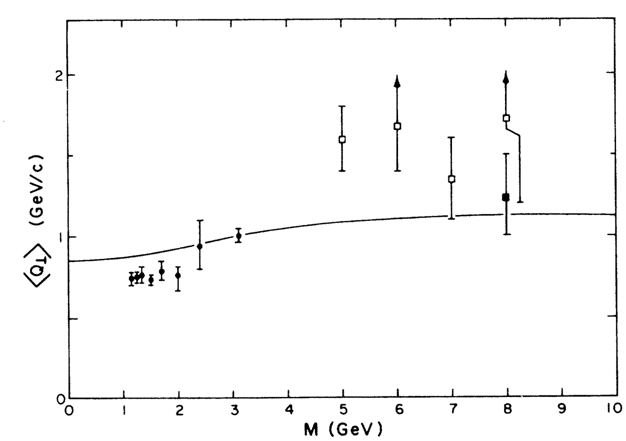

FIG. 12. Average transverse momentum of muon pairs versus muon pair mass. Compared with the data of Anderson *et al.* (Ref. 2) (●), Hom *et al.* (Ref. 1) (□), and L. Kluberg *et al.* [Phys. Rev. Lett. 37, 1451 (1976)] (■).

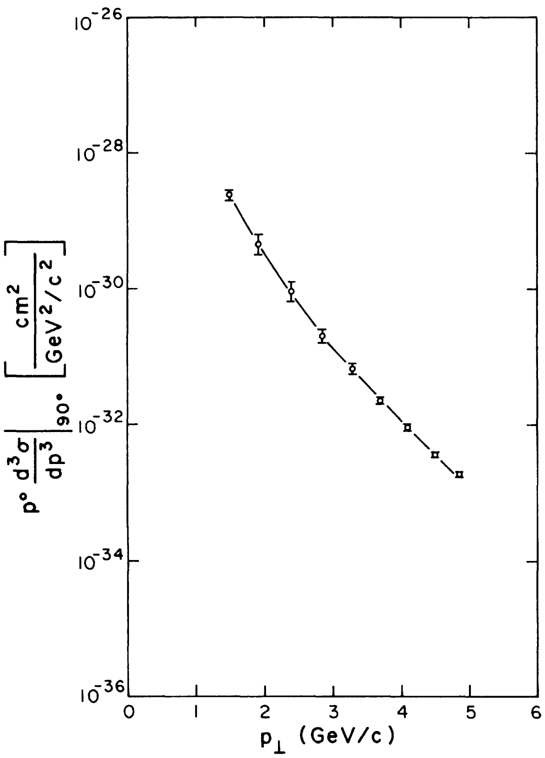

FIG. 13. $p^0 d^3\sigma/dp^3$ single-pion spectrum at 90° compared to the data of Eggert *et al*. (Ref. 13) at $\sqrt{s}=45.1$ GeV.

D. $<Q_\perp>$

Our calculation shows the rise of $\langle Q_\perp \rangle$ with Q^2 but saturates at $\langle Q_\perp \rangle \simeq 1.1$ GeV/c (Fig. 12).

E. Transverse-momentum pion spectrum

We have also calculated the single-particle spectrum of pions produced in pp collisions in this constituent-interchange model[15] utilizing the $\pi + q \to q + \pi$ quark-interchange subprocess (Fig. 2). We have included the $F_\pi(k^2)=A(-k^2+m^2)^{-1/2}$ form factor that gives the $p^0 d\sigma/dp^3 \propto A^4 p_\perp^{-8}$ behavior. Including colored quarks, there is a factor of $\frac{1}{9}$ entering this cross section, similar to the $\frac{1}{3}$ arising in the quark annihilation process for lepton pairs, Eq. (2.1). The data[13] for π^0 produced at 90° with $\sqrt{s}=45.1$ GeV are fitted in Fig. 13 with $A=12.8$. The value of A^2 determined from the lepton-pair spectrum is thus consistent with that needed to fit the pion spectrum in the constituent-interchange model.

F. Conclusions

We conclude that the constituent-pion–quark scattering model for lepton pair production including form factors can account for the dependence of the continuum produced single-lepton and lepton-pair spectra in transverse and longitudinal momentum and in the lepton-pair mass. It also accounts for the relative normalization of pion- versus proton-produced lepton-pair data, and is consistent with the constituent-interchange-model normalization for single-pion production.

---

*Work supported in part by the National Science Foundation.

[1]D. C. Hom *et al*., Phys. Rev. Lett. 37, 1374 (1976).

[2]K. J. Anderson *et al*., Phys. Rev. Lett. 37, 799 (1976).

[3]K. J. Anderson *et al*., sumitted to XVIII International Conference in High Energy Physics, Tbilisi, USSR, 1976 (unpublished).

[4]J. P. Boymond *et al*., Phys. Rev. Lett. 33, 112 (1974).

[5]S. D. Drell and T. M. Yan, Phys. Rev. Lett. 25, 316 (1970).

[6]M. Duong-van, K. V. Vasavada, and R. Blankenbecler [Phys. Rev. D 16, 1389 (1977)] use a similar approach but with scalar partons. We use spin-$\frac{1}{2}$ quarks and therefore require the form factor. We additionally calculate the single-lepton spectra, the lepton pair spectra in bins not containing resonances, and the spectra with incident pion beams.

[7]G. Chu and J. F. Gunion, Phys. Rev. D 10, 3672 (1974).

[8]J. F. Gunion, Phys. Rev. D 14, 1400 (1976).

[9]See for example, Eq. (2.11) of Riazuddin and B. W. Lee, Phys. Rev. 146, 1202 (1966).

[10]M. Fontannaz, Phys. Rev. D 14, 3127 (1976).

[11]M. Duong-van, Phys. Lett. 60B, 287 (1976).

[12]R. D. Field and R. P. Feynman, Phys. Rev. D 15, 2590 (1977).

[13]K. Eggert *et al*., Nucl. Phys. B98, 49 (1975).

[14]The Boymond data at $\sqrt{s}=24$ GeV have been determined to be too low by a factor of 1.4. If we allow for this correction, then

$$A^2=(1.4)\,(7.8)^2=(9.2)^2.$$

See P. A. Piroué, in *Particles and Fields* '76; proceedings of the Annual Meeting of the Division of Particles and Fields of the APS, edited by H. Gordon and R. F. Peierls (BNL, Upton, New York, 1977), p. A1.

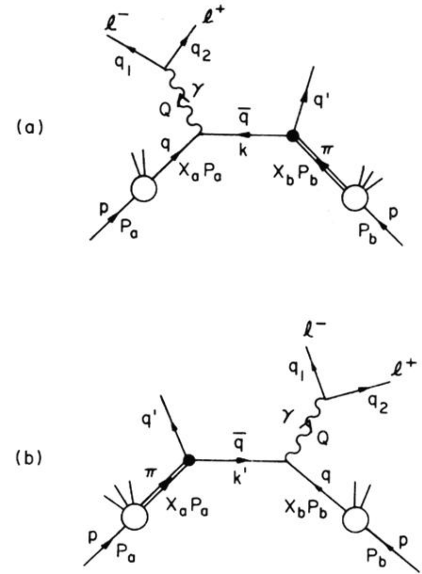

FIG. 1. (a) Direct and (b) crossed diagrams for $pp \to l^+ l^- X$ via secondary-pion–quark scattering with quark interchange.

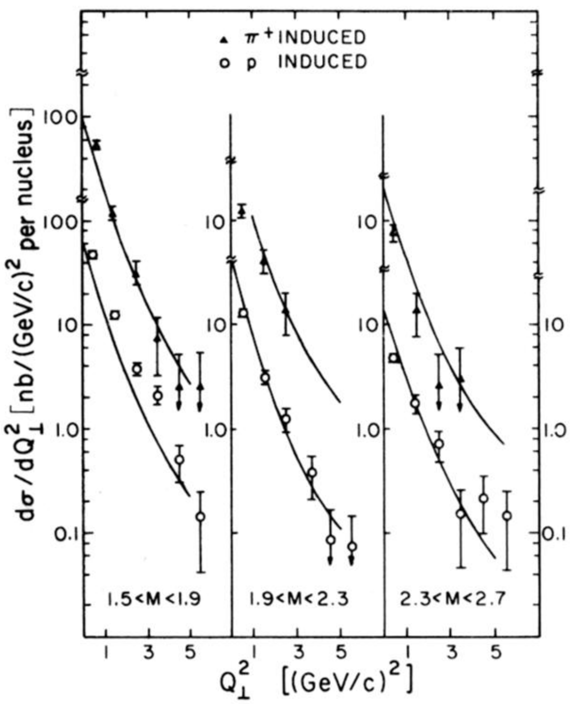

FIG. 10. $d\sigma/dQ_{\perp}{}^{2}$ for muon pairs, per nucleus, for a carbon target, for both incident proton and π^{+} beams. Compared with the data of Anderson *et al*. (Ref. 3) at $\sqrt{s}=20.6$ GeV in various mass bins.

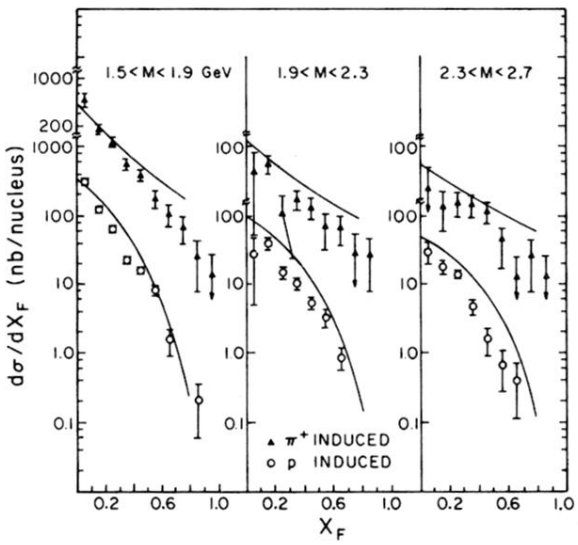

FIG. 11. $d\sigma/dx_F$ for muon pairs, per nucleus, for a carbon target, for both incident proton and π^+ beams. Compared with the data of Anderson *et al*. (Ref. 3) at $\sqrt{s} = 20.6$ GeV in various mass bins.

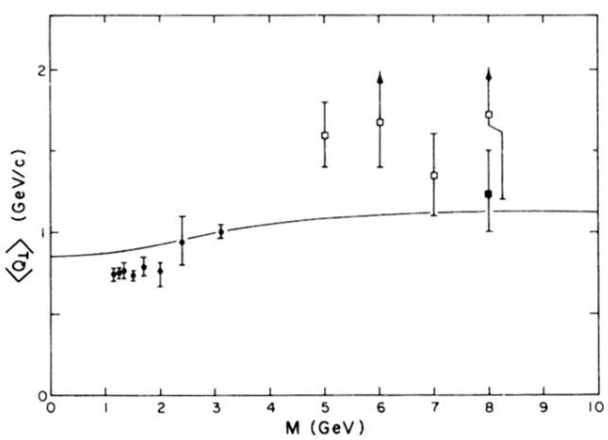

FIG. 12. Average transverse momentum of muon pairs versus muon pair mass. Compared with the data of Anderson *et al.* (Ref. 2) (●), Hom *et al.* (Ref. 1) (□), and L. Kluberg *et al.* [Phys. Rev. Lett. 37, 1451 (1976)] (■).

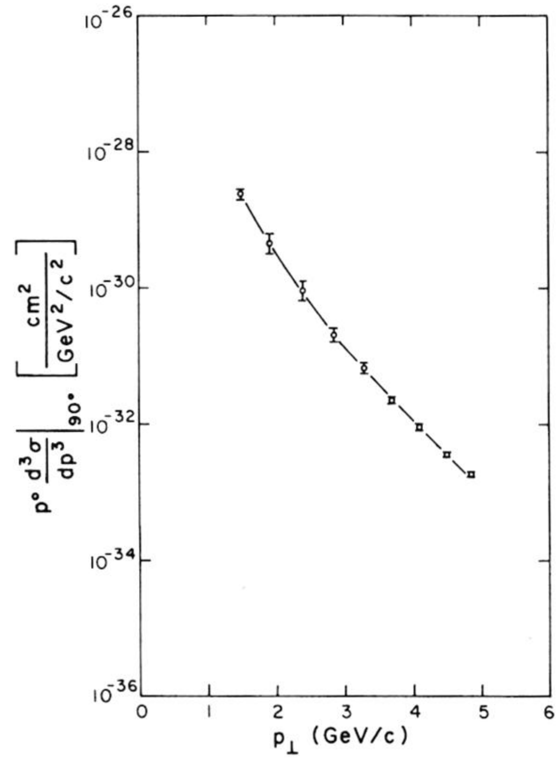

FIG. 13. $p^0 d^3\sigma/dp^3$ single-pion spectrum at 90° compared to the data of Eggert *et al*. (Ref. 13) at $\sqrt{s} = 45.1$ GeV.

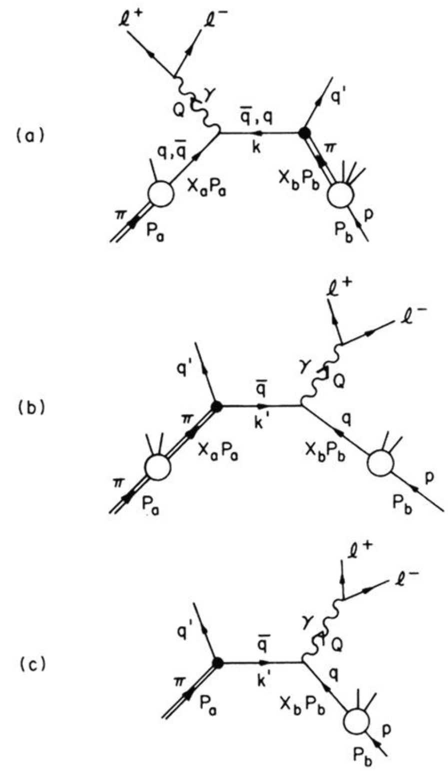

FIG. 2. (a) Direct and (b) crossed diagrams for secondary-pion–quark scattering for pion beams in $\pi p \to l^+ l^- X$ and (c) initial-pion diagram.

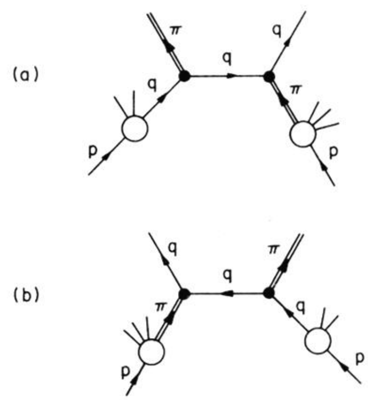

FIG. 3. Direct and crossed diagrams for secondary-pion–quark scattering in $pp \to \pi X$ via constituent interchange.

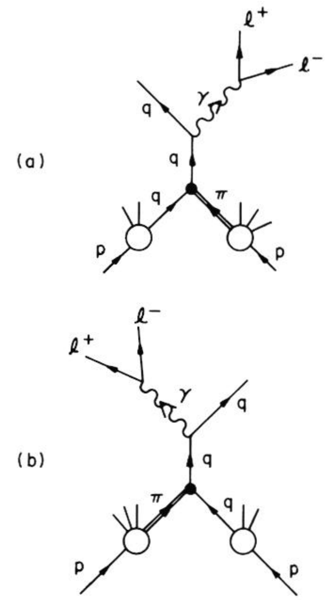

FIG. 4. Quark bremsstrahlung or s-channel quark diagrams for $pp \to l^+ l^- X$ via secondary-pion–quark scattering.

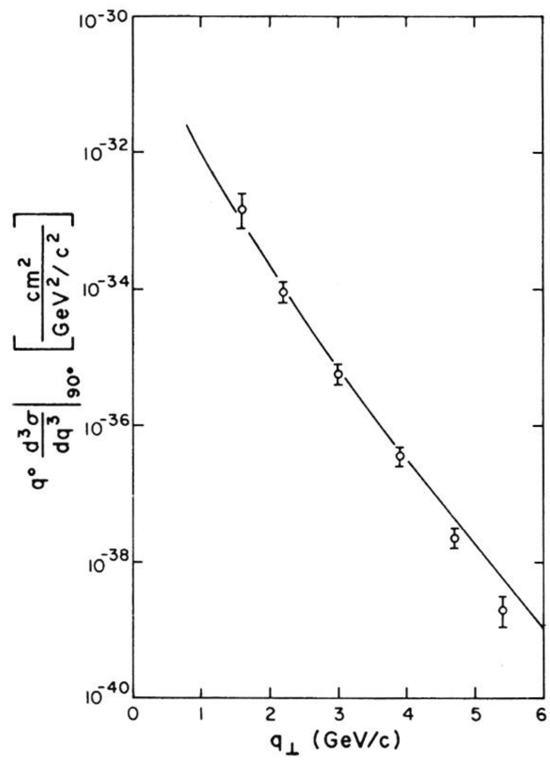

FIG. 5. $q^0 d^3\sigma/dq^3$ for single muons at 90° compared to the data of Boymond *et al*. (Ref. 4) at $\sqrt{s} = 23.7$ GeV.

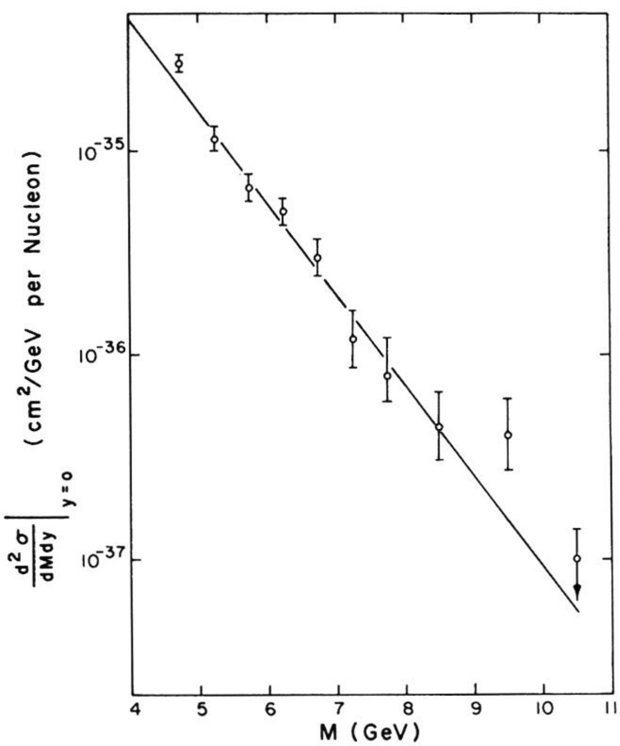

FIG. 6. $d^2\sigma/dMdy$ for muon pairs at $y=0$ compared to the data of Hom *et al*. at $\sqrt{s}=27.4$ GeV.

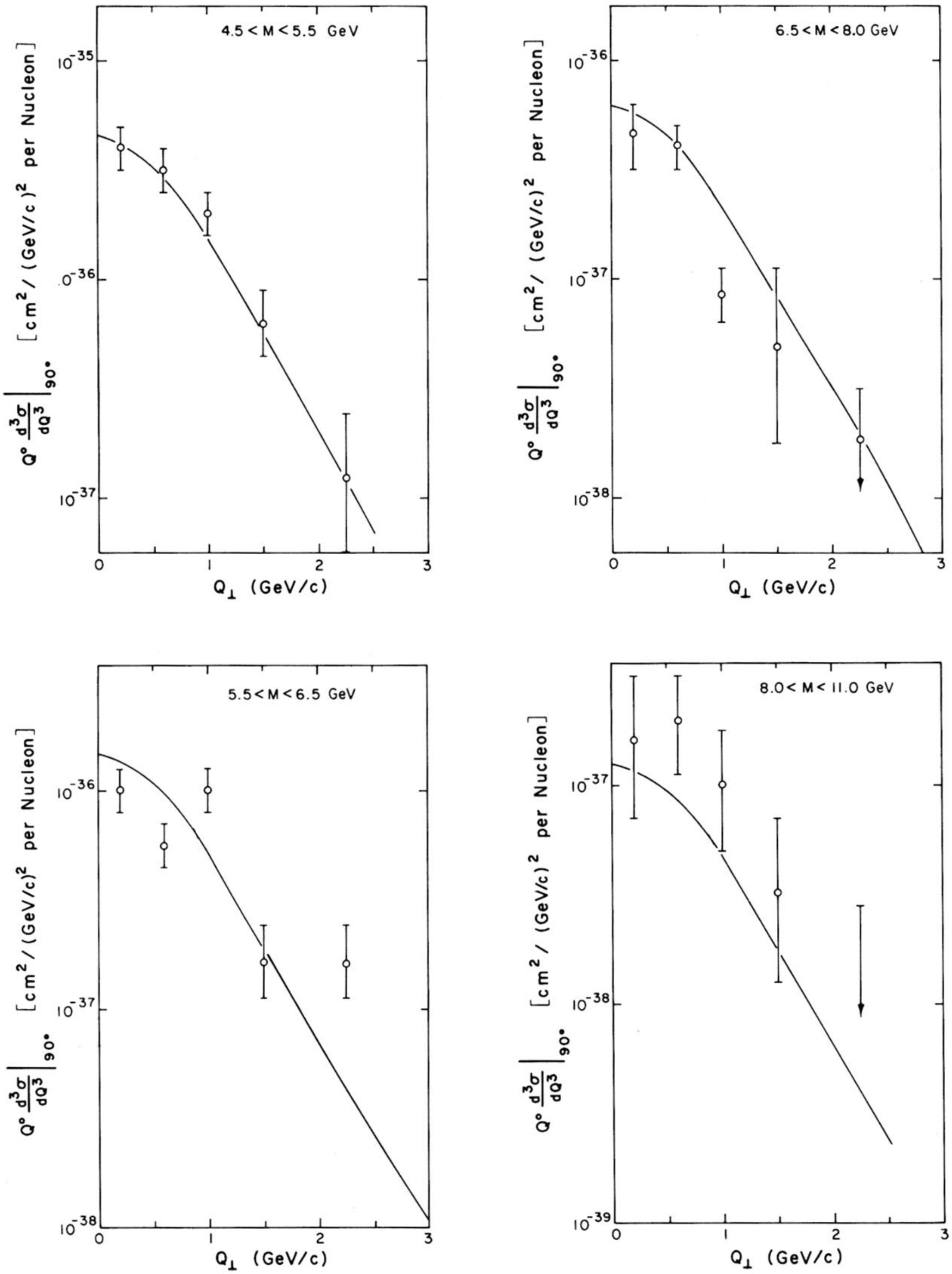

FIG. 7. $Q^0 d^3\sigma/dQ^3$ for muon pairs at 90° and $\sqrt{s} = 27.4$ GeV. Compared to the data of Hom *et al*. (Ref. 4) for various mass bins.

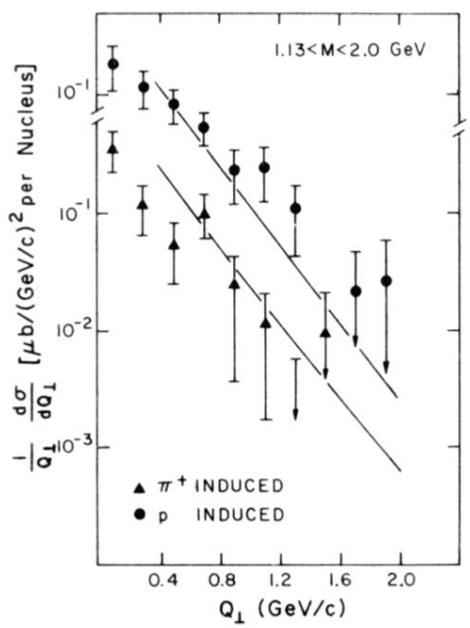

FIG. 8. $Q_\perp^{-1} d\sigma/dQ_\perp$ for muon pairs, per nucleus, for a Be target, for both incident proton and π^+ beams. Compared with the data of Anderson *et al.* (Ref. 2) at $\sqrt{s} = 16.8$ GeV in a nonresonant mass bin.

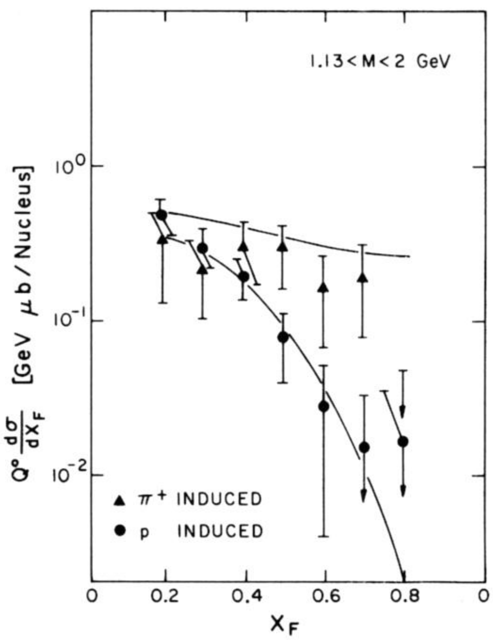

FIG. 9. $Q^0 d\sigma/dx_F$ for muon pairs, per nucleus, for a Be target, for both incident proton and π^+ beams. Compared with the data of Anderson *et al*. (Ref. 2) at $\sqrt{s} = 16.8$ GeV in a nonresonant mass bin.